Physica D 411 (2020) 132603

Contents lists available at ScienceDirect

Physica D

journal homepage: www.elsevier.com/locate/physd

Ensemble-based method for the inverse Frobenius–Perron operator problem: Data-driven global analysis from spatiotemporal "Movie" data

Naratip Santitissadeekorn [a,*], Erik M. Bollt [b]

[a] Department of Mathematics, University of Surrey, Guildford, Surrey, UK
[b] Clarkson University, Potsdam, NY, USA

ARTICLE INFO

Article history:
Received 6 December 2019
Received in revised form 20 May 2020
Accepted 1 June 2020
Available online 3 June 2020
Communicated by B. Hamzi

Keywords:
Frobenius–Perron operator
Inverse problem
Transfer operator
Coherent structures
Aggregate data

ABSTRACT

Given a sequence of empirical distribution data (e.g. a movie of a spatiotemporal process such as a fluid flow), this work develops an ensemble data assimilation method to estimate the transition probability that represents a finite approximation of the Frobenius–Perron operator. This allows a dynamical systems knowledge to be incorporated into a prior ensemble, which provides sensible estimates in instances of limited observation. We demonstrate improved estimates over a constrained optimization approach based on a quadratic programming problem. The estimated transition probability then enables several probabilistic analysis of dynamical systems. We focus only on the identification of coherent patterns from the estimated Markov transition to demonstrate its application as a proof-of-concept. To the best of our knowledge, there have not been many works on data-driven methods to identify coherent patterns from this type of data. While here the results are presented only in the context of dynamical systems applications, this work we present here has the potential to make a contribution in wider application areas that require the estimation of transition probabilities from a time-ordered spatio-temporal distribution data.

1. Introduction

This work focuses on an ensemble-based technique to estimate a Markov transition matrix, which is a finite approximation of the Frobenius–Perron (or transfer) operator, from a sequence of empirical distribution data. For instances, in a fluid experiment where droplets of dye are introduced into the fluid surface and their evolution is recorded as a sequence of images or in some PIV imagery, a sequence of a large number of "unlabelled particles" are recorded, in which case it would be difficult or even infeasible to track individual particle trajectory. However, these particles can be aggregated (perhaps after experiments) to provide empirical distribution data. In particular, the conditional transition probability of the transition matrix is estimated and the ensemble of these parameters can be used to understand the uncertainty of the estimate as well. The algorithm in this work modifies the formulation of the ensemble Kalman filter (EnKF) but it is not used in the filtering application. Instead, the entire data is used at once for the estimation and, EnKF is iteratively applied to improve the estimate; hence iterative EnKF (IEnKF). This approach is a Bayesian framework in nature, so the prior ensemble of the parameters is updated according to Bayes' rule to obtain the posterior ensemble. The flexibility of prior ensemble construction can be critical to obtaining realistic results in the case where available data is non-informative. Recent works with a similar goal [1,2] have studied the approximation of the transition matrix in the context of the so-called inverse Frobenius–Perron problem [3] where the estimated transition matrix is subsequently used to reconstruct the underlying one-dimensional map. The estimation method is simply a gradient-based constraint optimization. However, the approach in [1,2] was demonstrated only for a specific set of initial distributions, each of which is highly concentrated on individual Markov state, instead of arbitrary distributions. The estimation of the Markov transition probability is also of interest in a wider context such as econometric where the estimation problem is set up to allow for the quadratic programming [4–6]. A fully Bayesian approach was developed in [7] assuming that the rows of the transition matrix are independently distributed as the Dirichlet distribution. The posterior distribution is, however, analytically intractable. The structure of such a prior is also restrictive in the sense that the covariance between any two elements in the same row is always negative. Since the number of parameters is N^2 for N Markov states, it can be practically infeasible to use a sampling method such as Markov chain Monte Carlo in this fully Bayesian setting. Therefore, uncertainty analysis

* Corresponding author.
E-mail address: n.santitissadeekorn@surrey.ac.uk (N. Santitissadeekorn).

https://doi.org/10.1016/j.physd.2020.132603
0167-2789/

is usually ignored and only the posterior mode is computed by solving a constrained nonlinear equation using, for example, a nonlinear programming approach. Note that in the limit of "large" samples, an approximation of the covariance matrix is available but for a large number of Markov states, the number of available observations is usually too small to be considered as large samples.

In obtaining an estimated transition matrix, several probabilistic analyses of the data are made possible. For example, it allows an identification of coherent patterns (e.g. [8–12]), an approximation of transition probabilities from a basin to another (e.g. the stochastic basin hopping in [13,14] or computation of probabilistic transport pathway [15]. This work will focus only on the application of coherent structure or pattern identification. Understanding large-scale persistent patterns or coherent structures emerging from a chaotic dynamical system has been a subject of research interest since it is fundamental to gain insight both quantitatively and qualitatively into a study of transport problems. Thus several advanced algorithms to extract the large-scale persistent structure have been developed. Most recent algorithms are either geometric-based techniques [16–24], which rely on advanced theories of Lagrangian manifolds, or set-oriented methods, which can be considered as probabilistic approaches [8–12,25]. In cases where equations of the underlying dynamical system are known or their (numerical) approximations are available, Lagrangian coherent structures, which are transport barriers roughly moving along with the flow, can be constructed from analytic geometric-based methods based on theoretical concepts such as lobe dynamics, finite-time material manifolds, shape coherence, and braiding. On the other hand, the set-oriented methods use transfer operator (or Frobenius–Perron operator) theories to identify a large-scale almost invariant set for autonomous or periodic systems or finite-time coherent sets for non-autonomous systems, which minimizes transport across their boundaries. An extensive comparison between the two approaches as well as highlights of recent applications can be found in [26].

In some situations, however, theoretical or computational models are not available. When only spatio-temporal observational data is available, coherent structures have to be inferred based solely on relevant data. Numerous works have been proposed to extract coherent structures from the Lagrangian trajectory data such as a collection of trajectories of ocean drifters. In [13,22,27–31], the coherent structures are motivated by the finite-time coherent sets represented by the eigenvector of the Frobenius–Perron operator, which are shown to approximately minimize the conditional probability of the transport in and out of the coherent sets. A variety of data-driven methods are used in these works such as those motivated by spectral clustering [22,27,29,30], diffusion map method [28], and finite-element methods [31]. In [32,33], the coherent structures are the slow-dynamics mode of the Koopman operator, which is the adjoint of the Frobenius–Perron operator. To our best knowledge, however, this is the first study that uses empirical distribution (or aggregate) data to infer coherent structures.

2. Background

2.1. Approximation of Frobenius–Perron operator

This section briefly describes a basic formulation of the Frobenius–Perron operator approximation and how it can be used to find the coherent sets associated with an autonomous, deterministic dynamical system on a bounded domain. Thus the notion of coherent sets is simplified to the almost invariant sets as studied by several works [10,12,34,35]. A generalization to the stochastically perturbed autonomous system or non-autonomous systems is given in [11,31]. However, we will focus only on the simplified case, which is adequate to provide a formulation of the problem required to demonstrate our main contribution.

Consider a discrete-time dynamical system on a bounded set $\Sigma \subset \mathbf{R}^d$

$$z_{n+1} = \Phi(z_n), \tag{2.1}$$

where $\Phi : \Sigma \to \Sigma$ is a measurable and non-singular transformation. A concrete example of Φ will be given as part of our numerical experiments in the subsequent sections. If our knowledge of z_n is described by a probability density $f_n \in L^1(\Sigma)$, the Frobenius–Perron operator $\mathcal{F}$ associated with Φ is given by

$$f_{n+1}(z_{n+1}) := \mathcal{F} f_n = \int_\Sigma \delta(z_{n+1} - \Phi(z_n)) f_n(z_n) dz_n, \tag{2.2}$$

where δ is the Dirac delta function and serves as a (deterministic) transition kernel in this context. The Ulam–Galerkin method seeks a finite-dimensional approximation of $\mathcal{F}$ in a form of $r \times r$ Markov transition matrix $\mathbf{P}$ over the r-disjoint cells $\Sigma_r = \{R_1, \ldots, R_r\}$ such that $\Sigma = \bigcup_{i=1}^r R_i$. Note the Frobenius–Perron operator can be represented exactly by a finite-state Markov transition matrix if Φ is a piecewise-linear and expanding semi-Markov map. The ith row and jth column element (denoted by p_{ij}) of $\mathbf{P}$ can be probabilistically interpreted as a conditional probability that $x_{n+1} \in R_j$ given that $x_n \in R_i$. The Ulam approximation uses a finite sample $Z_n = \{z_n^{(1)}, \ldots, z_n^{(N_z)}\}$, in which $z_n^{(k)} \in R_i$, to approximate p_{ij} by

$$p_{ij} \approx \frac{\#\{\Phi(Z_n^{(k)}) \in R_j\}}{N_z}, \tag{2.3}$$

where $\#\{\Phi(Z_n^{(k)}) \in R_j\}$ counts the number of points of $\Phi(Z_n^k) \in R_j$. The projection of f_n onto the finite basis function $\{\Xi_j(R_j)\}_{j=1}^r$ and give $f_n \approx \{q_1(n), \ldots, q_r(n)\}$ where

$$q_j(n) = \int_{R_j} f_n(z_n) dz_n. \tag{2.4}$$

Under the above approximation, the evolution of $q(n) = [q_1(n), \ldots, q_r(n)]$ follows a linear equation $q(n+1) = \mathbf{P}q(n)$, which gives an approximation $f(n+1) \approx q_{n+1}$.

The above discretization introduces an error into the approximation of $\mathcal{F}$ in a way that $\mathbf{P}$ would be "closer" to the following operator:

$$\mathcal{F}_\epsilon f_n = \int_\Sigma K(x - \Phi(y)) f_n(y) dy, \tag{2.5}$$

where $K(x - \Phi(y))$ is a stochastic transition kernel, satisfying $K \geq 0$ almost everywhere and $\int_\Sigma K(x - \Phi(y)) dy = 1$. An in-depth discussion of this error can be found in [10]. The clustering problem in this context then aims to find a finite union of sets in Σ_r, say A, such that $\Phi^{-1}(A) \approx A$. We use the spectral partitioning method in [10] in this work to identify A. In what follows, we will describe a data-driven reconstruction of $\mathbf{P}$ in the case that Φ is unavailable and the available data is a time-ordered empirical distribution.

2.2. Problem statement

Motivated by the Galerkin–Ulam approximation, we are interested in a discrete-time, r-state first-order Markov chain $x(t)$ for $t = 0, 1, \ldots, T$ associated with a $(r \times r)$ transition probability matrix $\mathbf{P}$ whose the element p_{ij} describes a constant conditional

probability associated with a change from state s_i to s_j for $i, j = 1, \ldots, r$. Thus p_{ij} satisfies the following conditions:

$$0 \le p_{ij} \le 1, \quad \sum_j p_{ij} = 1. \tag{2.6}$$

We will refer to the above inequality restrictions as the "non-negativity" condition (despite the upper bound) and the equality constraint as the "sum-to-one" condition. They will also be collectively referred to as the Markov restriction. The unconditional probability of $x(t)$ is denoted by

$$q_j(t) := Pr(x(t) = s_j), \tag{2.7}$$

and the dynamic of $q_j(t)$ follows the recursive equation

$$q_j(t) = \sum_i p_{ij} q_i(t-1). \tag{2.8}$$

Therefore, at a given time t, we may consider $x(t)$ as a multinomial random variable with the probability of "success" $q_j(t)$.

If we are given sample paths of N repeated sample (i.e. sequences of states where $x(t)$ visit at $t = 0, \ldots, T$), we have an access to the number of individuals for which $x(t-1) = s_i$ and $x(t) = s_j$, denoted by $n_{ij}(t)$. In some applications, $n_{ij}(t)$ may not always be available and only the sample aggregate proportion for each time t are known, i.e., only

$$y_j(t) = \sum_i n_{ij}(t) / \sum_i \sum_k n_{ik}(t). \tag{2.9}$$

It is clear that $\sum_j y_j(t) = 1$. The time-ordered sequence $y_j(t)$ for $j = 1, \ldots, r$ and $t = 0, 1, \ldots, T$ will be called **proportion data**.

Suppose we have a $(r \times 1)$ vector of the time-ordered proportion data

$$\mathbf{y}(t) = [y_1(t), y_2(t), \ldots, y_r(t)]' \in S^r, \tag{2.10}$$

where S^r denotes the $r-1$ dimensional simplex. It will be assumed that the time-series data $y_j(t)$ is a sample of $q_j(t)$ generated by an unknown transition probabilities that are assumed to be constant over the entire sample period. Therefore, this work aims at a reconstruction of p_{ij} based on $\mathbf{y}(t)$.

3. Ensemble least squares framework

3.1. Basic setup

To estimate the transition matrix, we make the following model assumption:

$$y_j(t) = \sum_i y_i(t-1) p_{ij} + \epsilon_j(t), \quad t = 0, 1, \ldots, T-1, \tag{3.1}$$

where the error from replacing the unconditional probabilities $q_j(t)$ in (2.8) by proportion data $y_j(t)$ is accounted for by a random variable $\epsilon_j(t)$. We assume that $E[\epsilon_j] = 0$, $Var[\epsilon_j] = \sigma_j^2$ and $E[\epsilon_i \epsilon_j] = 0$ for $i \neq j$, hence the name "independent scheme". The model (3.1) can be expressed as a linear model using the following notations: $\mathbf{y}_j = [y_j(1), y_j(2), \ldots, y_j(T)]'$ is a $(T \times 1)$ vector of the observed proportion of the state j, $\mathbf{p}_j$ is a $(r \times 1)$ vector of the jth column of the unknown transition matrix $\mathbf{P}$, $\boldsymbol{\epsilon}_j = [\epsilon_j(1), \epsilon_j(2), \ldots, \epsilon_j(T)]'$ is a $(T \times 1)$ vector of random perturbation and X_j is the $(T \times r)$ matrix given by

$$X_j = [\mathbf{y}(0) \quad \mathbf{y}(1) \cdots \mathbf{y}(T-1)]', \tag{3.2}$$

where $\mathbf{y}(t)$ is defined in (2.10). Note that $X_1 = X_2 = \cdots = X_r$. For any $j = 1, \ldots, r$, the linear model based on the relation (3.1) is separately given by

$$\mathbf{y}_j = X_j \mathbf{p}_j + \boldsymbol{\epsilon}_j \quad j = 1, \ldots, r. \tag{3.3}$$

Without a constraint on $\mathbf{p}_j$, the solution of (3.3) can be easily obtained by the least-square method, which yields the minimizing solution of the normal equation

$$\tilde{\mathbf{p}}_j = (X_j' X_j)^\dagger X_j' \mathbf{y}_j, \tag{3.4}$$

where $(X_j' X_j)^\dagger$ is the pseudo-inverse of $(X_j' X_j)$. Note that we only have to solve for $\tilde{\mathbf{p}}_j$ for each $j = 1, \ldots, r-1$ in isolation and then deduce $\tilde{\mathbf{p}}_r$ from the sum-to-one constraint. This solution, however, neglects the non-zero correlation between p_{ij} for each fixed i required as a result of the sum-to-one condition.

To generalize (3.3) to allow for a correlation structure, the equation systems (3.3) are first combined into the following form:

$$\underbrace{\begin{bmatrix} \mathbf{y}_1 \\ \mathbf{y}_2 \\ \vdots \\ \mathbf{y}_{r-1} \end{bmatrix}}_{:=\mathbf{y}} = \underbrace{\begin{bmatrix} X_1 & & & \\ & X_2 & & \\ & & \ddots & \\ & & & X_{r-1} \end{bmatrix}}_{:=X} \underbrace{\begin{bmatrix} \mathbf{p}_1 \\ \mathbf{p}_2 \\ \vdots \\ \mathbf{p}_{r-1} \end{bmatrix}}_{:=\mathbf{p}} + \underbrace{\begin{bmatrix} \boldsymbol{\epsilon}_1 \\ \boldsymbol{\epsilon}_2 \\ \vdots \\ \boldsymbol{\epsilon}_{r-1} \end{bmatrix}}_{:=\epsilon}. \tag{3.5}$$

This gives a linear system

$$\mathbf{y} = X\mathbf{p} + \boldsymbol{\epsilon}, \tag{3.6}$$

where X is a $((r-1)T \times (r-1)r)$ matrix. We assume that $E[\boldsymbol{\epsilon}] = 0$ and $E[\boldsymbol{\epsilon}\boldsymbol{\epsilon}'] = \mathbf{R}$ is a $((r-1)T \times (r-1)T)$ observation covariance matrix. Note that the rth term is suppressed to deal with the inherent collinearity due to the sum-to-one restriction. The estimate of $\mathbf{p}_r$ is readily obtained from that of $\mathbf{p}$ and the sum-to-one restriction. In general, another component instead of the rth component can be suppressed. This raises an obvious issue that the estimate may not be the same for a different choice of the suppressed component. For example, if $\mathbf{y}_r(0) \gg \mathbf{y}_j(0)$ for $j = 1, \ldots, r-1$, the suppression of $\mathbf{y}_r$ as in (3.5) may lead to a significant loss of information of underlying p_{ij}. Therefore, a choice of the suppressed state must be carefully made; if $\mathbf{y}_i(t) \ll \mathbf{y}_j(t)$ for all $i \neq j$ at any time t, suppression of the ith state would be reasonable. Thus, the suppression of rth component in (3.5) is arbitrary (as long as keeping in mind the above comment) since the permutation of the states does not alter the Markov Chain.

We consider the estimate that minimizes the cost function

$$\phi(\mathbf{p}) = (\mathbf{y} - X\mathbf{p})' \mathbf{R}^{-1} (\mathbf{y} - X\mathbf{p}) + (\mathbf{p} - \mathbf{p}^o)' \mathbf{B}^{-1} (\mathbf{p} - \mathbf{p}^o), \tag{3.7}$$

where $\mathbf{p}^o$ is an initial guess of $\mathbf{p}$ and the $((r-1)r \times (r-1)r)$ covariance matrix $\mathbf{B}$ gives a prior covariance structure between p_{ij} and $\mathbf{R}$ is a $((r-1)T \times (r-1)T)$ covariance matrix of $\mathbf{y}$. Note that the cost function (3.7) can also be written by

$$\phi(\mathbf{p}) \propto \frac{1}{2} \mathbf{p}' (X' \mathbf{R}^{-1} X + \mathbf{B}^{-1}) \mathbf{p} + (X' \mathbf{R}^{-1} \mathbf{y} + \mathbf{B}^{-1} \mathbf{p}^o) \mathbf{p}. \tag{3.8}$$

Without the Markov constraints on $\mathbf{p}$, the generalized least squares solution for (3.7) is given by

$$\mathbf{p}^* = \mathbf{p}^o + \mathbf{B} X' (X \mathbf{B} X' + \mathbf{R})^{-1} (\mathbf{y} - X\mathbf{p}^o). \tag{3.9}$$

Thus, the least squares solution is confined within the subspace spanned by the basis vectors of $\mathbf{B}$. Since $\mathbf{y}$ is a proportion data, we may assume that $\mathbf{R}$ has the covariance structure of a multinomial distribution. For the current arrangement of the vector $\mathbf{y}$, $\mathbf{R}$ has the following structure:

$$\mathbf{R} = \begin{bmatrix} \mathbf{R}_{1,1} & \mathbf{R}_{1,2} & \cdots \mathbf{R}_{1,r-1} \\ \vdots & \ddots & \vdots \\ \mathbf{R}_{r-1,1} & \mathbf{R}_{r-1,2} & \cdots \mathbf{R}_{r-1,r-1} \end{bmatrix}, \tag{3.10}$$

where $\mathbf{R}_{i,i}$ is a $T \times T$ diagonal matrix with $\alpha y_i(t)(1-y_i(t))$ for $t = 1, \ldots, T$ on the diagonal, $\mathbf{R}_{i,j}$ is a $T \times T$ diagonal matrix with $-\alpha y_i(t) y_j(t)$ on the diagonal for some $0 < \alpha < 1$.[1]

We assume that each row of the transition matrix is independent and has a Dirichlet prior distribution. Under the current arrangement of the vector $\mathbf{p}$, $\mathbf{B}$ will have $(r-1)^2$ diagonal-blocks $\mathbf{B}_{i,j}$ for $i, j = 1, \ldots, r-1$, each of which has a size of $(r \times r)$. Denote the Dirichlet parameter for the l−th row of the transition matrix by $[a_{l,1}, \ldots, a_{l,r}]$. Let $a_{l,0} = \sum_{i=1}^{r} a_{l,i}$. The sub-block $\mathbf{B}_{i,i}$ is a diagonal matrix with elements $a_{k,i}(1-a(k,i))/(a_{k,0}+1)$ for $k = 1, \ldots, r$. The sub-block $\mathbf{B}_{i,j}$ for $i \neq j$ is diagonal with elements $-a_{k,i}a_{k,j}/(a_{k,0}+1)$ for $k = 1, \ldots, r$.

In general, the optimal solution (3.9) may not satisfy the Markov restriction. A constrained optimization approach such as quadratic programming may be used instead based on the cost function (3.8), which requires computation of $\mathbf{R}^{-1}$ and $\mathbf{B}^{-1}$. If $\mathbf{R}$ is chosen as above, the inversions can be derived analytically as explained in Appendix A. If we require $[a_{l,1}, \ldots, a_{l,r}]$ to be the same for all l (i.e. using the same Dirichlet parameters for all rows), $\mathbf{B}$ can be analytically inverted in a similar manner.

Alternatively, we can address the issue of the Markov restriction by using the additive log ratio (alr) transformation:

$$h_{ij} := alr(p_{ij}) = \ln p_{ij} - \ln p_{ir}, \qquad i = 1, \ldots, r, j = 1, \ldots, r-1. \tag{3.11}$$

Thus we have a nonlinear observation operator

$$\mathbf{y} = \mathcal{H}(\mathbf{h}) := X \circ alr^{-1}(\mathbf{h}), \tag{3.12}$$

where the element of the vector $\mathbf{h}$ is arranged in the same order as $\mathbf{p}$ as described in (3.5) and the inverse transformation alr^{-1} is given by

$$p_{ij} = alr^{-1}(h_{ij}) = \frac{e^{h_{ij}}}{1+\sum_{k=1}^{r-1} e^{h_{ik}}}, \qquad i = 1 \ldots, r, k = 1 \ldots, r-1. \tag{3.13}$$

The element p_{ir} can be obtained by $p_{ir} = 1 - \sum_{j=1}^{r-1} p_{ij}$. The cost function in term of $\mathbf{h}$ is given by

$$\varphi(\mathbf{h}) = (\mathbf{y} - \mathcal{H}(\mathbf{h}))' \mathbf{R}^{-1} (\mathbf{y} - \mathcal{H}(\mathbf{h})) + (\mathbf{h} - \mathbf{h}^o)' \mathbf{S}^{-1} (\mathbf{h} - \mathbf{h}^o). \tag{3.14}$$

If $\mathcal{H}(\mathbf{h})$ is linearized at the point $\mathbf{h}^o$, the optimal solution of the linearized system of (3.14) over the subspace spanned by a set of basis vector Ψ such that $\Psi\Psi' = \mathbf{S}$ is

$$\mathbf{h}^* = \mathbf{h}_o + \Psi \mathbf{V}' (\mathbf{V}\mathbf{V}' + \mathbf{R})^{-1} (\mathbf{y} - \mathcal{H}(\mathbf{h}^o)), \tag{3.15}$$

where $\mathbf{V} = H\Psi$ is a $(r-1)T \times (r-1)r$ matrix and H is the $(r-1)T \times (r-1)r$ Jacobian matrix of $\mathcal{H}$ evaluated at $\mathbf{h}^o$. For the alr transformation, the Jacobian $\mathcal{H}$ can be exactly computed. In addition, with the linearized system H the choice of $\mathbf{h}^o$ and S can be statistically inspired. If we assume that the prior term is normally distributed as $N(\mathbf{h}^o, \mathbf{S})$, the posterior distribution of $\mathbf{h}$ will then be $N(\mathbf{h}^*, \mathbf{S}^a)$, where

$$\mathbf{S}^a = (H' \mathbf{R}^{-1} H + \mathbf{S}^{-1})^{-1}. \tag{3.16}$$

Note that if $\mathcal{H}(\mathbf{h})$ is linearized at a point $\mathbf{h}^f \neq \mathbf{h}^o$, the optimal solution is

$$\mathbf{h}^* = \mathbf{h}_o + \Psi \mathbf{V}' (\mathbf{V}\mathbf{V}' + \mathbf{R})^{-1} (\mathbf{y} - \mathcal{H}(\mathbf{h}^o)) + \mathbf{S}^a \mathbf{S}^{-1} (\mathbf{h}^o - \mathbf{h}^f). \tag{3.17}$$

[1] The random process governing how observations are created is described by the multinomial experiment leading to (2.9). However, if the number of trials and $q_j(t)$ as defined in (2.8) are unknown, we must make some assumptions to approximate the variance and covariance of the observation process. We make a simplification by using $y_j(t)$ instead of $q_j(t)$. Also, if we were to know the number of trials, we would then use it for α^{-1}. However, we lack this knowledge in practice, so we arbitrary choose $0 < \alpha < 1$ instead.

A brief description of the derivation of (3.17) is given in Appendix B. The formulation (3.17) could potentially increase a significant computational expense relative to (3.15). Thus, our work will focus only on (3.15). In the next section, we will describe an ensemble-based approach that adopts (3.15) to iteratively update the ensemble. This approach will allow us to circumvent the derivation of the H in general cases; hence enabling a gradient-free algorithm. It also provides an assessment of uncertainty around the estimate through the sample covariance.

3.2. Ensemble-based algorithm

We now consider an ensemble-based algorithm that approximates the solution of (3.14) through sample statistics. The key idea in this section follows closely the "stochastic" formulation of the ensemble Kalman filter (EnKF) developed for data assimilation problem [36]. Other formulations such as Ensemble transform Kalman filter (ETKF) [37] or Ensemble Adjustment Kalman filter (EAKF) [38], which can be classified as a "deterministic" formulation, are also possible for a similar development but our development below will be pivoted to the stochastic EnKF.

Suppose that we have an ensemble such that each of its members will be denoted by $\mathbf{h}_e^{(i)}$ for $i = 1, \ldots, N_e$, where N_e is the number of ensemble members. We can construct a $r(r-1) \times N_e$ matrix of scaled deviation

$$\mathbf{H}_e = \frac{1}{\sqrt{N_e - 1}} [\mathbf{h}_e^{(1)} - \bar{\mathbf{h}}_e, \ldots, \mathbf{h}_e^{(N_e)} - \bar{\mathbf{h}}_e], \tag{3.18}$$

where $\bar{\mathbf{h}}_e$ is the ensemble mean, i.e., $\bar{\mathbf{h}}_e = N_e^{-1} \sum_{j=1}^{N_e} \mathbf{h}_e^{(j)}$. We assume that $\bar{\mathbf{h}}_e \approx \mathbf{h}_o$. Also, we assume that the covariance matrix $\mathbf{S}$ in (3.15) is approximately given by

$$\mathbf{S} \approx \mathbf{S}_e = \mathbf{H}_e \mathbf{H}_e'. \tag{3.19}$$

In light of (3.15), we wish to assimilate observation $\mathbf{y}$ to construct a new ensemble from the initial ensemble such that the new ensemble mean would satisfy the following map:

$$\bar{\mathbf{h}}_e^* = \bar{\mathbf{h}}_e + \mathbf{H}_e \mathbf{V}_e' (\mathbf{V}_e \mathbf{V}_e' + \mathbf{R})^{-1} (\mathbf{y} - \mathcal{H}(\bar{\mathbf{h}}_e)), \tag{3.20}$$

where $\mathbf{V}_e = H\mathbf{H}_e$ is a $(r-1)T \times N_e$ matrix. It is clear that the update term in (3.20) is pre-multiplied by $\mathbf{H}_e$, so the update term is confined to the subspace spanned by the column of $\mathbf{H}_e$ (i.e. the initial guess ensemble). In other words, the algorithm lacks necessary information to update any terms that has a non-zero projection onto the space orthogonal to the column space $\mathbf{H}_e$. This issue can be difficult to avoid in a large-dimensional problem where the ensemble size tends to be much less than the dimension of the problem. Nevertheless, the above update gives the optimal solution in the subspace spanned by $\mathbf{H}_e$, but in general not optimal in the model space.

The formulation (3.20) still needs a computation of the Jacobian H of $\mathcal{H}$. To obtain a full ensemble-based algorithm, we want to approximate this by an ensemble of the predicted observation $\mathbf{y}_e^{(i)} = \mathcal{H}(\mathbf{h}_e^{(i)})$. To this end, let $\bar{\mathbf{y}}_e$ be the ensemble mean and $\mathbf{Y}_e$ be a $T(r-1) \times N_e$ matrix of scaled deviation constructed as in (3.18). If we make a linear approximation $\mathbf{Y}_e \approx \mathbf{V}_e$ and $\bar{\mathbf{y}}_e \approx \mathcal{H}(\bar{\mathbf{h}}_e)$, we may update each ensemble member by

$$\mathbf{h}_e^{*(i)} = \mathbf{h}_e^{(i)} + \mathbf{H}_e \mathbf{Y}_e' (\mathbf{Y}_e \mathbf{Y}_e' + \mathbf{R})^{-1} (\mathbf{y} - \mathbf{y}_e^{(i)}), \tag{3.21}$$

where the new ensemble mean will approximate the desired ensemble mean in (3.20). It follows that the new matrix of scaled deviation, denoted by $\mathbf{H}_e$ satisfies

$$\mathbf{H}_e^* = (I - \mathbf{K}_e X)\mathbf{H}_e, \tag{3.22}$$

where $\mathbf{K}_e = \mathbf{H}_e \mathbf{Y}_e' (\mathbf{Y}_e \mathbf{Y}_e' + \mathbf{R})^{-1}$. Thus, the new ensemble covariance matrix is given by

$$\mathbf{S}_e^* = (\mathbf{I} - \mathbf{K}_e X)\mathbf{S}_e (\mathbf{I} - \mathbf{K}_e X)', \tag{3.23}$$

which is considered to be too small by a factor of $(\mathbf{I} - \mathbf{K}_e X)$ if compared with the theoretical covariance $\mathbf{S}_e^* = (\mathbf{I} - \mathbf{K}_e X)\mathbf{S}_e$ found from the Bayesian principle for normal inference of population mean.

To address this inconsistency, the so-called Ensemble Kalman filter (EnKF) used the virtual observation in the innovation instead of the actual observation to correct the underestimate covariance matrix. In particular, it replaces $\mathbf{y} - \mathbf{y}_e^{(i)}$ in (3.21) by $\mathbf{y}^{(i)} - \mathbf{y}_e^{(i)}$, where $\mathbf{y}^{(i)}$ is randomly drawn from a distribution with mean $\mathbf{y}$ and covariance $\mathbf{R}$. In this paper, we will draw a virtual observation $\mathbf{y}^{(i)}(t)$ independently for $i = 1 \ldots, N_e$ at each time $t = 0, \ldots, T$ from a Dirichlet distribution with a parameter vector $\alpha(y_1(t), \ldots, y_r(t))$. The factor $0 < \alpha < 1$ is used to control the magnitude of variance and covariance of the distribution. Given the virtual observation $\mathbf{y}^{(i)}$, we may construct the scale deviation matrix based on $\mathbf{y}^{(i)}$, called $\mathbf{R}_s$ such that $\mathbf{R} \approx \mathbf{R}_s\mathbf{R}_s'$. We can also avoid a construction of the matrix $\mathbf{R}$ by replacing it with its ensemble approximation and rewrite (3.21) by

$$\mathbf{h}_e^{*(i)} = \mathbf{h}_e^{(i)} + \mathbf{H}_e\mathbf{Y}_e'(\mathbf{Y}_e\mathbf{Y}_e' + \mathbf{R}_s\mathbf{R}_s')^{-1}(\mathbf{y}^{(i)} - \mathbf{y}_e^{(i)}). \tag{3.24}$$

There is another advantage of using $\mathbf{R}_s$ in (3.24) to reduce computational workload, which will be discussed in the subsequent section. The above estimation is repeated iteratively until the outcome stabilizes under a stopping criterion; the new ensemble at the $k-$th iterative step becomes an initial ensemble for the $(k+1)$th. The iteration may be stopped when a norm of the relative discrepancy of the two successive estimates is less than a given threshold.

In general, the solution in (3.15) and the ensemble mean of (3.24) can be very different. When using (3.15), the matrix S has to be designed on the alr-coordinate, i.e., eliciting the correlation structure of $\mathbf{h}$ instead of $\mathbf{p}$. However, it is difficult to determine the correlation of $\mathbf{h}$ due to a lack of possible distributions on the alr-coordinate. This issue is circumvented in the ensemble approach in which the ensemble can be drawn for $\mathbf{p}$ (e.g. from Dirichlet distribution) and then alr-transformed to an ensemble of $\mathbf{h}$ without a need for linearization of $\mathcal{H}$. The sample covariance can then be used instead of $\mathbf{S}$. To deal with this issue of implementing (3.15), we first determine $\mathbf{p}^o$ and obtain $\mathbf{h}^o$ through alr transformation and then assume $\mathbf{S}$ to have a correlation structure of the Dirichlet distribution with parameters $\mathbf{h}^o$. However, $\mathbf{h}^o$ and $\mathbf{S}$ constructed this way may not agree with the initial sample of the ensemble approach, i.e., $\mathbf{h}^o$ can be different from the sample mean and $\mathbf{S}$ may not even have the same structure as the sample covariance in general.

3.3. Implementation

The inversion in (3.21) is the main computational cost. To allow for computational feasibility in a large-scale problem, we make an approximation that $Y_e\mathbf{R}_s' \approx 0$ (i.e. Y_e is nearly orthogonal to $\mathbf{R}_s$). This approximation is reasonable on the ground that as long as our random sample of $\mathbf{h}_e^{(i)}$ is independent of the sample $\mathbf{y}^{(i)}$, $H_e\mathbf{R}_s'$ will tend to zero for a large ensemble size, so does $Y_e\mathbf{R}_s'$, following on the above comments led us to (3.21). With this approximation in mind, we have

$$(\mathbf{Y}_e\mathbf{Y}_e' + \mathbf{R}) = (\mathbf{Y}_e\mathbf{Y}_e' + \mathbf{R}_s\mathbf{R}_s') \approx (\mathbf{Y}_e + \mathbf{R}_s)(\mathbf{Y}_e + \mathbf{R}_s)'. \tag{3.25}$$

We can find the singular value decomposition (SVD) $\mathbf{Y}_e + \mathbf{R}_s = U\Lambda V'$ and the required pseudo-inverse of $(\mathbf{Y}_e\mathbf{Y}_e' + \mathbf{R})$ is approximated by

$$(\mathbf{Y}_e\mathbf{Y}_e' + \mathbf{R})^{-1} = U(\Lambda\Lambda')^{-1}U'. \tag{3.26}$$

In practice, the ensemble size tends to be much smaller than the total number of observations, so we usually have $N_e \ll T(r-1)$. Therefore, this approximation avoids a large computer storage and matrix product of $\mathbf{Y}_e\mathbf{Y}_e'$, which can, in general, be non-sparse. More importantly, it reduces an inversion of an $T(r-1)\times T(r-1)$ matrix to a computation of SVD for an $T(r-1)\times N_e$, where the former requires $O((T(r-1))^3)$ and the latter requires only $O((T(r-1))^2N_e)$. The update equation (3.21) now becomes

$$\mathbf{h}_e^{*(i)} = \mathbf{h}_e^{(i)} + \mathbf{H}_e\mathbf{Y}_e'U(\Lambda\Lambda')^{-1}U'(\mathbf{y}^{(i)} - \mathbf{y}_e^{(i)}). \tag{3.27}$$

It is easy to check that the largest matrix required to be stored to implement (3.27) is of the size $r(r-1)\times N_e$. For a very large r, the required memory access can be a practical concern that cannot be overlooked.

Several iterative schemes have also been studied for various implementation of EnKF. We follow the simple iteration as first used [39], where stochastic EnKF was applied iteratively to combat a strong nonlinearity in their reservoir engineering problem. Theoretical aspects of this approach in the context of regularization have been recently studied in [40]. In some practical applications, e.g. considered by Emerick and Reynolds [41], the observation error covariance matrix (i.e. $\mathbf{R}$ in our context) is inflated by the number of iterations to avoid overfitting in the experiment where ground-truth posterior density is accessible through the Metropolis–Hasting sampler and the observation error is normal. In Sakov [42,43], the ensemble-based formulation is developed via a linearization at a point $\mathbf{h}^f \neq \mathbf{h}^o$ as explained in (3.17) and the observation error covariance matrix is inflated in the same fashion suggested by [41]. This change, however, requires a user to use one of the deterministic versions of EnKF instead of the stochastic formulation. In [44], a comparison between the implementation of [41] and [42] approaches in the context of the bio-irrigation has recently shown an improved result when using [41]. It also explains in [44] why the method in [42] tends to stop updating ensemble after just a few iterations, which can lead to a poor result in some cases. In [45], iterative ETKF was employed based on a "residual nudging" method which requires the computationally expensive task of approximating a Jacobian of the nonlinear observation operator.

4. Numerical experiments

Two numerical experiments are carried out in the subsequent sections. We will use the Hellinger distance to quantify the difference between two discrete probability measures. It is given by

$$h(w_1, w_2) = \frac{1}{\sqrt{2}}\left\|\sqrt{w_1} - \sqrt{w_2}\right\|_2. \tag{4.1}$$

The constant term is used for scaling so that the Hellinger distance varies between 0 and 1. In what follows, we evaluate the error for each row of the estimated transition matrix and report an average of all rows of the transition matrix.

4.1. Toy problem

In this test experiment, the ground truth is a 16×16 Markov transition matrix (indexed by $\{1, \ldots, 16\}$) with a structure of nearly two 8×8 diagonal sub-matrices, see Fig. 1. The true distribution $q_i(t)$ is generated from the ground truth for $t = 0, 1, \ldots, 12$ with the initial distribution $q_i(0) = 1/2$ for $i = 2$ and $i = 15$ and zeros otherwise. The noisy test data at a time step t is then drawn from a multinomial distribution with parameters N_m and $q_i(t)$. The level of "noise" is therefore controlled by N_m where we examine two cases: $N_m = 10^5$ ("small" noise) and $N_m = 10^4$ ("large" noise). The random samples are then aggregated by averaging to produce noisy observation. To avoid dividing by zero when computing the inverse of $\mathbf{R}$ and $\mathbf{S}$, one sample is added to those Markov states without a sample from the above draw.

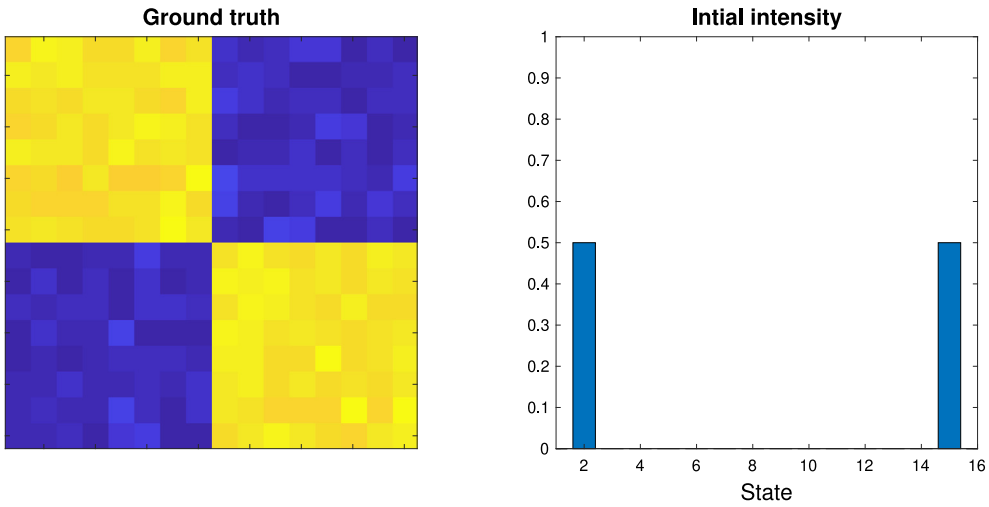

Fig. 1. Ground truth and true initial intensity for the toy problem in Section 4.1.

We compare the ensemble-based method (3.24), quadratic programming (3.8) under the Markov constraints and linearized approach (3.15). We use the ensemble mean as a point estimate of the ensemble-based method.

Initialization: We now explain the initialization of these methods.

- The ensemble method requires the initial ensemble of $\mathbf{p}$. For this experiment, we construct an initial ensemble by independently drawing an ensemble for each row of matrix with Dirichlet distribution with parameter $a_1 = a_2 = \cdots = a_{16} = 1$. That is our initial guess for each row is the uniform measure. The ensemble drawn for each row is then arranged into the format of $\mathbf{p}$ as described in (3.5). Each ensemble member is then alr-transformed into $\mathbf{h}$ as required by (3.24).
- The quadratic programming approach requires a prior guess $\mathbf{p}^o$ and $\mathbf{B}$. We can let $\mathbf{p}^o$ be the mean of the Dirichlet distribution used to initialize the ensemble approach. Thus, all elements of $\mathbf{p}$ is $1/16$. Similarly, $\mathbf{B}$ is a covariance matrix corresponding to the parameter $a_1 = a_2 = \cdots = a_{16} = 1$ arranged in the format explained in the previous section.
- For the linearized approach, $\mathbf{h}^o$ and $\mathbf{S}$ are required. To make the initial guess consistent with the ensemble approach, $\mathbf{h}^o$ is a zero-vector (i.e. all elements are zeros). It is unclear how to make $\mathbf{S}$ consistent with the initial sample covariance of $\mathbf{h}$. Nevertheless, we can insist $\mathbf{S}$ to have the structure of the covariance matrix of the Dirichlet distribution. In other words, $\mathbf{S}$ is the same as $\mathbf{B}$ used in the quadratic programming.

The virtual observations for (3.24) are drawn from the multinomial distribution using $\alpha = 1/N_m$. This implies that we have a rough understanding of the level of noise in the data but the exact knowledge of N_m is still assumed to be unknown. We compare errors based on the Hellinger distance for various methods in Fig. 2.

The ensemble-based estimate (for a large ensemble size $N_e = 6400$) shows smaller errors than the other methods. However, for this particular case, the error from the ensemble method increases for a smaller N_m (i.e. larger noise) while the errors for the other methods are nearly the same for both large and small noises. The error analysis with respect to the ensemble size is shown in Fig. 3. This shows that the "optimal" ensemble size, which provides substantially improved estimates, could be much larger than the number of parameters. Nevertheless, it is possible to have $N_e < r$ and still obtain an improved estimate over other methods.

An uncertainty analysis can also be investigated for the ensemble method using the prior and posterior sample covariance structures as shown in Fig. 4. To aid interpretability, the sample covariance matrix is permuted so that the entries are arranged in the following order,

$$p_{1,1}, p_{1,2}, \ldots, p_{1,16}, p_{2,1}, p_{2,2}, \ldots, p_{2,16}, \ldots, p_{16,1}, p_{2,16}, \ldots, p_{16,16}.$$

Thus, instead of having the structure similar to (3.10), the prior sample covariance has the block-diagonal structure indicating the independence between the rows of the transition matrix. It is clear that the ensemble approach updates the posterior sample covariance to allow correlations between the rows of the transition matrix, which agrees with the bi-partite structure of the ground truth. This structure, however, becomes less evident in the large-noise case. As pointed out above, the linearized approach (3.15) can also provide covariance structure through a normal assumption of the prior distribution of $\mathbf{h}$, see (3.16). However, as shown in Fig. 5, the covariance structure fails to capture the correlation induced by the block-diagonal structure of the ground truth, despite the correct block-diagonal structure shown in the estimated transition matrix. Therefore, when the initial ensemble is constructed from the simplex coordinate for $\mathbf{p}$ and transformed into the alr-coordinate, the ensemble method is not generally an approximation of (3.15).

4.2. Double-Gyre flow

Consider a double-gyre system on a bounded domain $\Omega = [0, 2] \times [0, 1]$

$$\begin{aligned} \frac{dx}{dt} &= A\pi \sin(\pi f(x,t)) \cos(\pi y) \\ \frac{dy}{dt} &= A\pi \cos(\pi f(x,t)) \sin(\pi y) \frac{df}{dx}, \end{aligned} \tag{4.2}$$

where $f(x,t) = \epsilon \sin(\omega t)x^2 + (1 - 2\epsilon \sin(\omega t))x$. For $\epsilon = 0$, the flow has a fixed separatrix $x = 1$ and the most dominant pattern is clearly the partition of Ω into two regions; one with $x \leq 1$ and the other with $x \geq 1$. For $\epsilon > 0$, the system is periodically perturbed and the demonstration of the dominant pattern can be found in [12]. We set $A = 0.25, \epsilon = 0.25, \omega = 2\pi$ to generate the test data. The domain Ω is subdivided into $N_x \times N_y$ uniform cells of size $\Delta x = 2/N_x, \Delta y = 1/N_y$. To generate the "true" transition matrix, 400 uniformly distributed tracers in each cell are propagated over 1 period and the transition probability from cell i to j (i.e. p_{ij}) is given by the proportion of initial tracers in

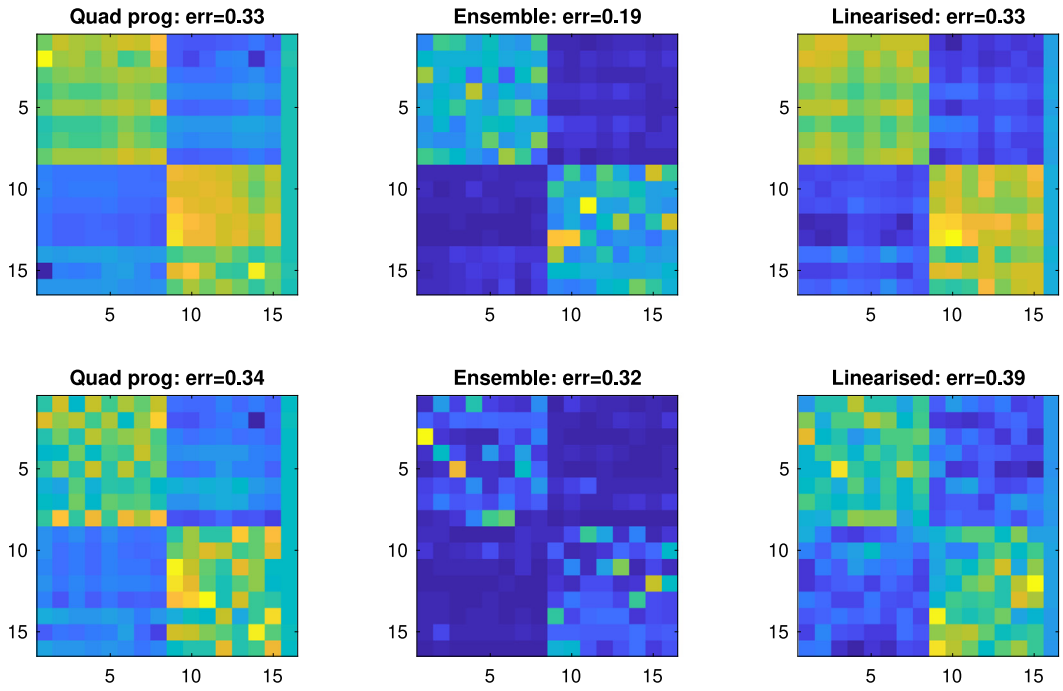

Fig. 2. Estimated transition matrix for various cases. The top row is the small noise case and the bottom row is the large noise case. The result of the ensemble approach is shown for the ensemble size of $N_e = 6400$.

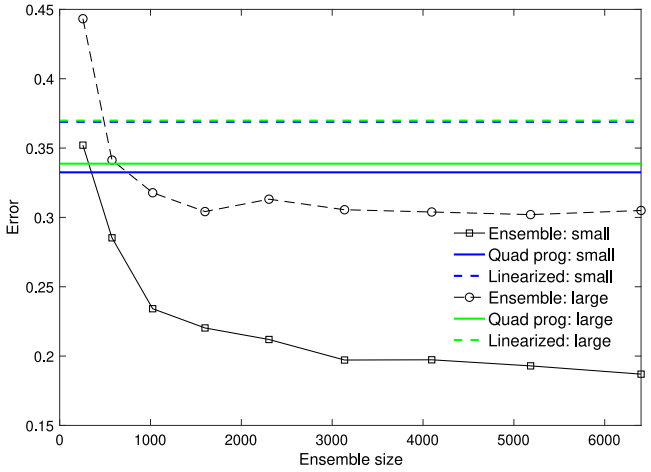

Fig. 3. Error analysis for varying ensemble sizes: $64K^2$ for $K = 1, 2, \ldots, 10$. The "small" and "large" in the data labels refer to the small and large noise cases, respectively.

cell i that goes to cell j after $t = 1$. A test data is generated by an evolution of the initial distribution as shown Fig. 6 under the test transition matrix over the time step $t = 0, 1, 2, \ldots, 10$. We test 3 different data set as illustrated in Fig. 6. The first initial distribution has non-zero regions in the three important places; left and right gyres and the separatrix. The second initial distribution focuses on the right and left gyres. The third initial distribution has non-zero regions on the left gyre only. As done in the preceding experiment, a noisy observation at each time step is aggregated from $N_m = 10^5$ random samples drawn from a multinomial distribution with the parameters based on the true test data.

The estimation of p_{ij} as the ensemble mean is shown in Figs. 7 and 9. The ensemble size is $N = 10{,}000$ and the ensemble is initialized to have an ensemble mean corresponding to the transition matrix of the unperturbed double-gyre flow; hence the dominant pattern of this matrix is just the partition by the vertical line $x = 1$. The results obtained from the ensemble approach are compared with those from the standard quadratic programming without a prior guess of the transition matrix. Fig. 7 clearly shows improved accuracy when using the ensemble-based method. In

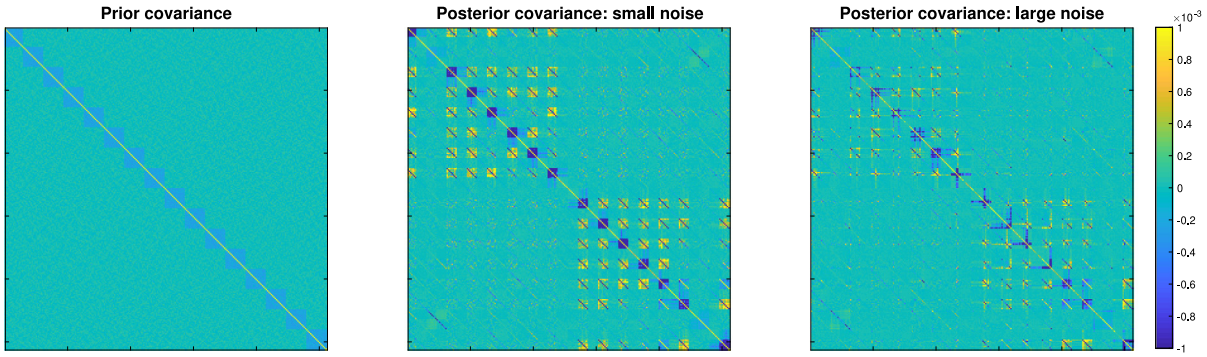

Fig. 4. Comparison between prior and posterior sample covariance for small and large noise experiments in the case of ensemble method (3.16). From the top of the matrix to the bottom, the entries correspond to $p_{1,1}, p_{1,2}, \ldots, p_{1,16}, p_{2,1}, p_{2,2}, \ldots, p_{2,16}, \ldots, p_{16,1}, p_{2,16}, \ldots, p_{16,16}$.

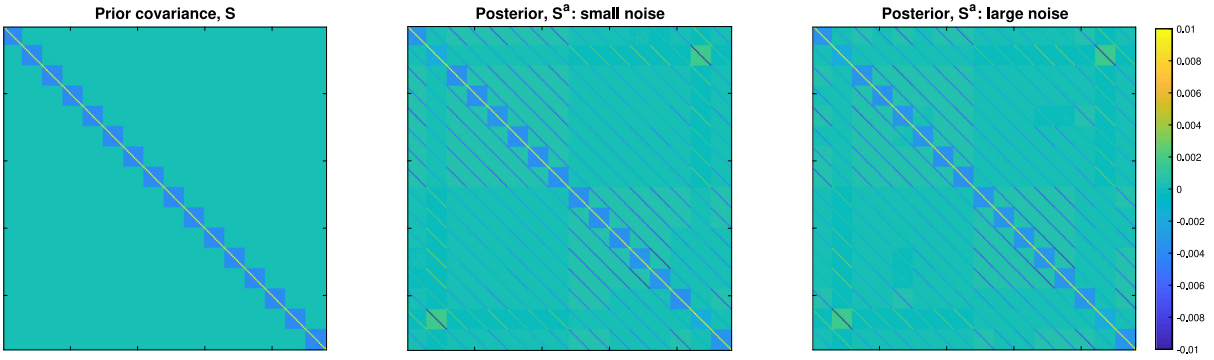

Fig. 5. Comparison between prior and posterior covariance for small and large noise experiments in the case of linearized system (3.16). From the top of the matrix to the bottom, the entries correspond to $p_{1,1}, p_{1,2}, \ldots, p_{1,16}, p_{2,1}, p_{2,2}, \ldots, p_{2,16}, \ldots, p_{16,1}, p_{2,16}, \ldots, p_{16,16}$.

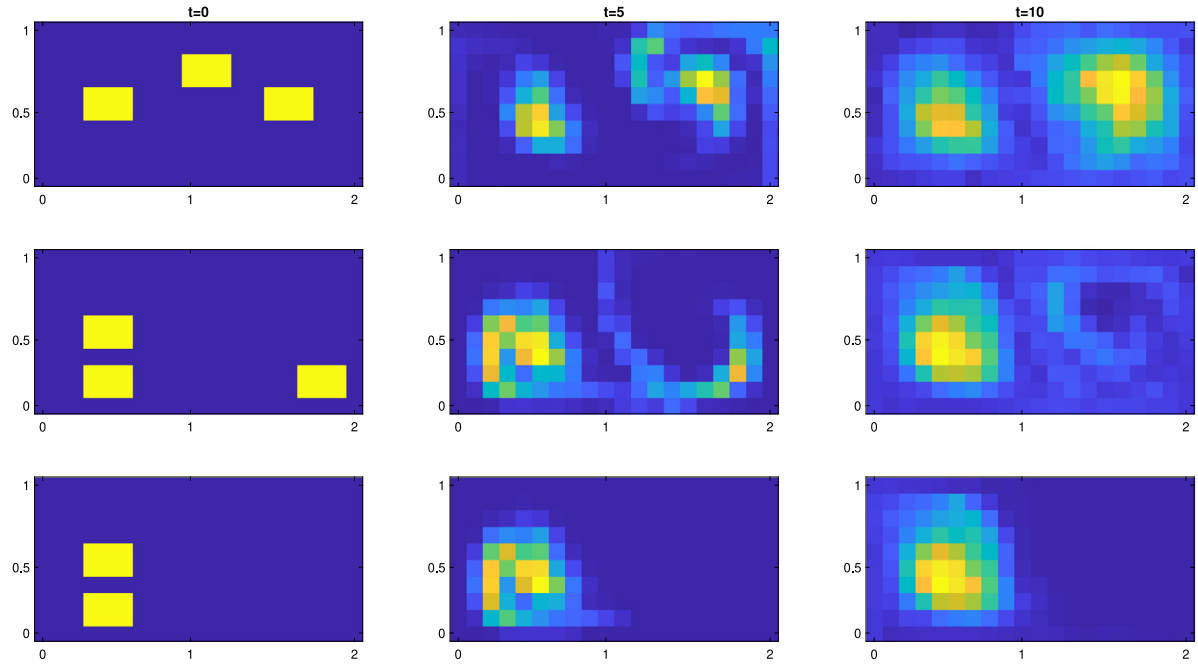

Fig. 6. From the top to bottom rows, the initial distributions of data set 1, 2, and 3 for the double gyre system and their corresponding evolutions at $t = 5$ and $t = 10$ are shown.

all cases, 6 numbers of the iteration are carried out and the error at each iteration is shown in Fig. 8.

After obtaining the estimate of the transition matrix $\mathbf{P}$, the inferred persistent pattern is computed based on the weighted principal component analysis. In particular, the second largest singular vector of the normalized transition matrix $\Pi\mathbf{P}$, where the diagonal elements of diagonal matrix Π is the stationary vector (i.e. the left eigenvector of $\mathbf{P}$ corresponding to the largest eigenvalue), are compared in Fig. 9 at the resolution of $N_x = 20, N_y = 10$. Note that the normalized matrix has the largest singular value of 1 with the uniform singular vector, see [12] for details.

For the data set 1, the ensemble approach reveals the "invariant island" that looks similar to the true pattern. However, the structure becomes vague in other data sets. The quadratic programming, however, provides the pattern that is nearly unchanged from the prior pattern in all cases. The results for other lower resolutions are quite similar (but not shown here).

We also investigate how the error changes with the resolution, see Fig. 10. Both errors of prior mean and the ensemble mean increase with the resolution at a similar rate. In other words, the error reduction ratio provided by the ensemble-based approach appears to be roughly constant for all resolutions. The variance reduction of the parameter p_{ij} (i.e. the ratio of the initial variance and variance after data assimilation) is shown in Fig. 11. Note that the top-left (bottom-right) submatrix corresponds to the left(right) gyre. The reduction of variance depends on the initial information in an intuitive way, see again Fig. 6. The first data set has fairly uniform variance reduction for all parameters while for the second data set the reduction is less achieved in the centre of the matrix, which is the gyre boundary area, and for the third data set the parameter corresponding to the right gyre gains even more significant variance due to the random walk model spreading out the ensemble in each iteration.

5. Conclusions and future works

This paper presents an ensemble-based method to estimate the transition matrix representation of a dynamical system through a time-series of proportion data. The algorithm takes into account the Markov constraints on the transition matrix via the ALR transformation. Based on the transformed variable, the ensemble-based algorithm then follows a similar formulation to the EnKF but it is applied iteratively to improve the estimate.

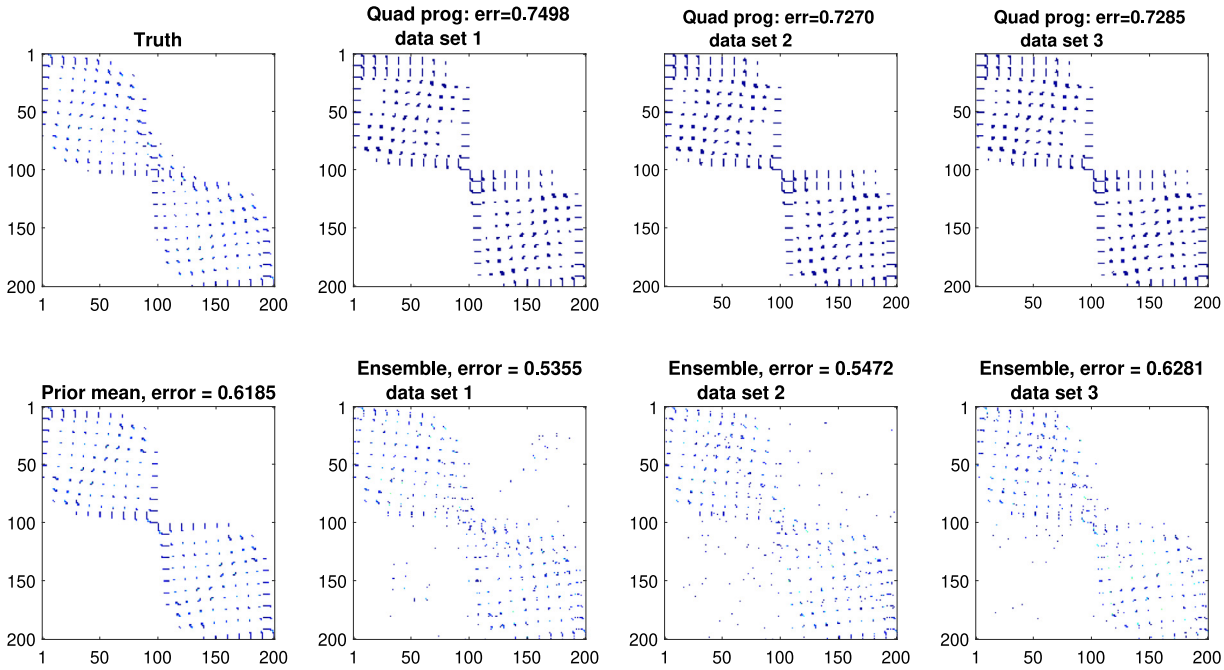

Fig. 7. The true transition matrix is generated from running the double-gyre system over 1 period using $N_x = 20$ and $N_y = 10$. The Prior mean is generated in the same way but using the unperturbed double-gyre flow. Estimates of the transition matrix are obtained by the quadratic programming as well as ensemble method for the dataset 1, 2 and 3.

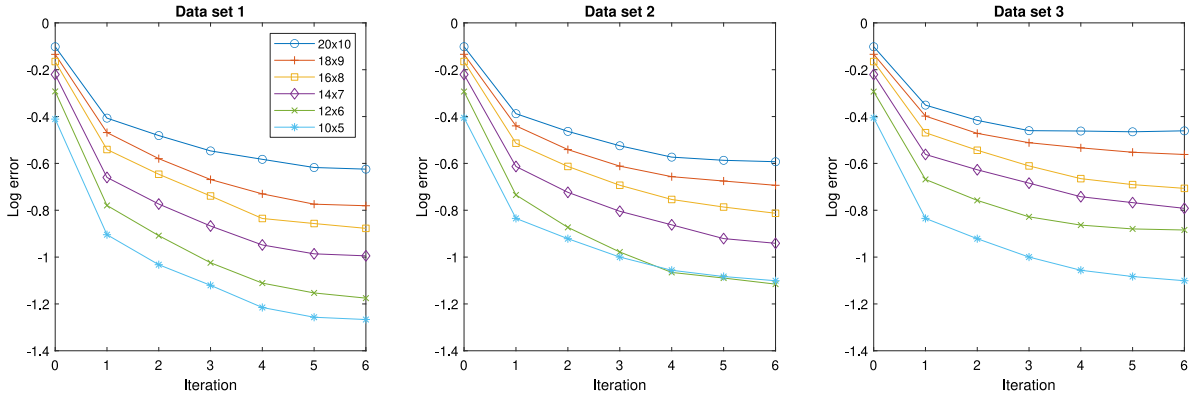

Fig. 8. The error (in the logarithmic scale) at each iteration for the dataset 1, 2 and 3 in the case of the ensemble method.

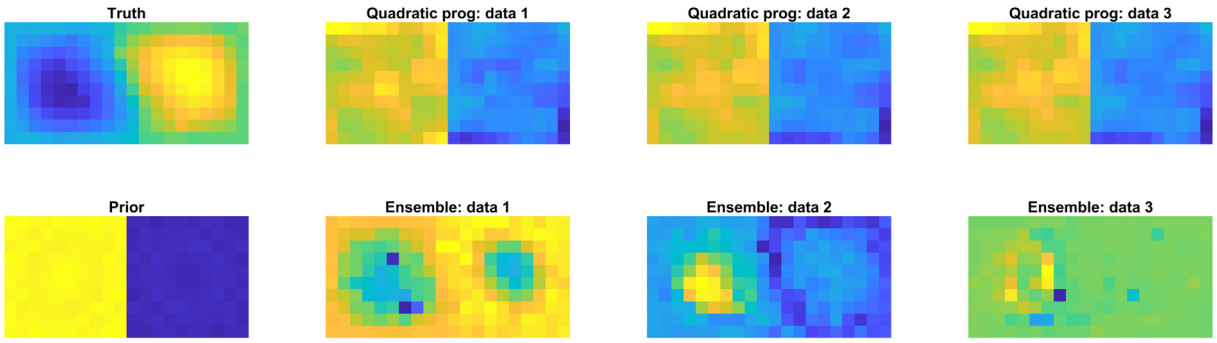

Fig. 9. Comparison of persistent patterns as the second singular vector of the normalized transition matrix, shown only for the case of $N_x = 20, N_y = 10$.

The ensemble-based approach in this work incorporates the prior knowledge of the matrix via the construction of the initial ensemble. The prior structure of the matrix can play a crucial role in achieving a realistic result for a large under-determined problem with noisy data. In our experiment with the double-gyre flow, a prior structure derived from the initial guess corresponding

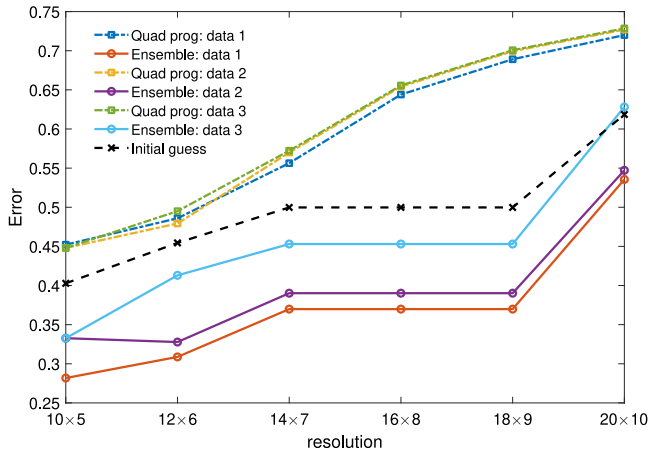

Fig. 10. Comparison of errors at various resolution.

to the unperturbed flow leads to an improved estimate of the transition matrix when compared with the estimate obtained from the standard quadratic programming without using any prior guess. The persistent pattern of the flow is also improved as a consequence. This approach also enables an approximated uncertainty analysis via the dispersion of ensemble (e.g. sample variance and covariance). Although the usefulness of the uncertainty is not extensively examined in the current work, it may be crucial in some applications. This approach can also be applied to real-world data available in the form of an image sequence, which can be considered as an evolution of aggregate data in some cases. The matrix representation that approximates the underlying flow can be of interest in many applications. For example, in a study of stochastic basin hopping, it will allow an approximation of the "exiting" probability from one basin to another. From a practical perspective, however, a high-resolution image may have to be sub-sampled into a low resolution due to a high computational cost of the algorithm. Our future work will also look into combining a dimensionality reduction technique with the current approach to reduce computational complexity. The key challenge in this direction is the required Markov constraint that has to be satisfied when making dimensionality reduction.

CRediT authorship contribution statement

Naratip Santitissadeekorn: Conceptualization, Methodology, Formal analysis, Visualization, Writing - original draft, Writing - review & editing. **Erik M. Bollt:** Conceptualization, Validation, Writing - review & editing.

Appendix A. Inversion of R and B

First we consider an inversion of a $(r-1)\times(r-1)$ matrix $\mathbf{C}$ of the following form:

$$\mathbf{C} = \begin{bmatrix} q_1(1-q_1) & -q_1q_2 & \cdots -q_1q_{r-1} \\ -q_2q_1 & q_2(1-q_2) & \cdots -q_2q_{r-1} \\ \vdots & \ddots & \vdots \\ -q_{r-1}q_1 & -q_{r-1}q_2 & \cdots q_{r-1}(1-q_{r-1}) \end{bmatrix}.$$

$$\mathbf{C}^{-1} = \begin{bmatrix} \frac{1}{q_r}+\frac{1}{q_1} & \frac{1}{q_r} & \cdots \frac{1}{q_r} \\ \frac{1}{q_r} & \frac{1}{q_r}+\frac{1}{q_2} & \cdots \frac{1}{q_r} \\ \vdots & \ddots & \vdots \\ \frac{1}{q_r} & \frac{1}{q_r} & \cdots \frac{1}{q_r}+\frac{1}{q_{r-1}} \end{bmatrix}.$$

To invert $\mathbf{R}$, we first note that we can permute $\mathbf{R}$ into a $(r-1)T\times(r-1)T$ block-diagonal matrix, called $\mathbf{D}$, that has T sub-blocks of size $(r-1)\times(r-1)$. In particular, if the $t-$th sub-block of $\mathbf{D}$, denoted by $D(t)$, is given by

$$\mathbf{D}(t) = \begin{bmatrix} y_1(t)(1-y_1(t)) & -y_1(t)y_2(t) & \cdots -y_1(t)y_{r-1}(t) \\ -y_2(t)y_1(t) & y_2(t)(1-y_2(t)) & \cdots -y_2(t)y_{r-1}(t) \\ \vdots & \ddots & \vdots \\ -y_{r-1}(t)y_1(t) & -y_{r-1}(t)y_2(t) & \cdots y_{r-1}(t)(1-y_{r-1}(t)) \end{bmatrix},$$

we take the (i,j) elements of each $\mathbf{D}(t)$ and expanding them into a $T\times T$ diagonal sub-block $\mathbf{R}_{i,j}$, see (3.10), in the order from 1 to T. Thus, we may write $\Pi_r\mathbf{D}\Pi_c = \mathbf{R}$ where Π_r and Π_c are permutation matrices corresponding to such a permutation. The above inversion formula given for $\mathbf{C}^{-1}$ can be used to find $\mathbf{D}(t)^{-1}$; hence $\mathbf{D}^{-1}$. It follows that $\Pi_c'\mathbf{D}^{-1}\Pi_r' = \mathbf{R}^{-1}$. Since $\mathbf{D}^{-1}$ has the same block-diagonal structure as $\mathbf{D}$ and $\mathbf{R}^{-1}$ are symmetric, we have $\Pi_r\mathbf{D}^{-1}\Pi_c = \mathbf{R}^{-1}$. In other words, we can rearrange the elements of $\mathbf{D}^{-1}$ to obtain $\mathbf{R}^{-1}$ in the same fashion that we rearrange elements of $\mathbf{D}$ to obtain $\mathbf{R}$. To sum up, we can invert $\mathbf{R}$ by

$$\mathbf{R}^{-1} = \begin{bmatrix} \mathbf{R}^{1,1} & \mathbf{R}^{1,2} & \cdots \mathbf{R}^{1,r-1} \\ \vdots & \ddots & \vdots \\ \mathbf{R}^{r-1,1} & \mathbf{R}^{r-1,2} & \cdots \mathbf{R}^{r-1,r-1} \end{bmatrix},$$

where $\mathbf{R}^{i,j}(k,k)$ for $i\neq j$ is a $T\times T$ diagonal matrix with the $k-$th diagonal elements

$$\mathbf{R}^{i,j}(k,k) = (\alpha y_r(k))^{-1} \qquad k=1,\ldots,T$$

and $\mathbf{R}^{i,i}(k,k)$ is also a $T\times T$ diagonal matrix with the $k-$th diagonal elements

$$\mathbf{R}^{i,i}(k,k) = \frac{1}{\alpha}\left(\frac{1}{y_r(k)}+\frac{1}{y_i(k)}\right) \qquad k=1,\ldots,T.$$

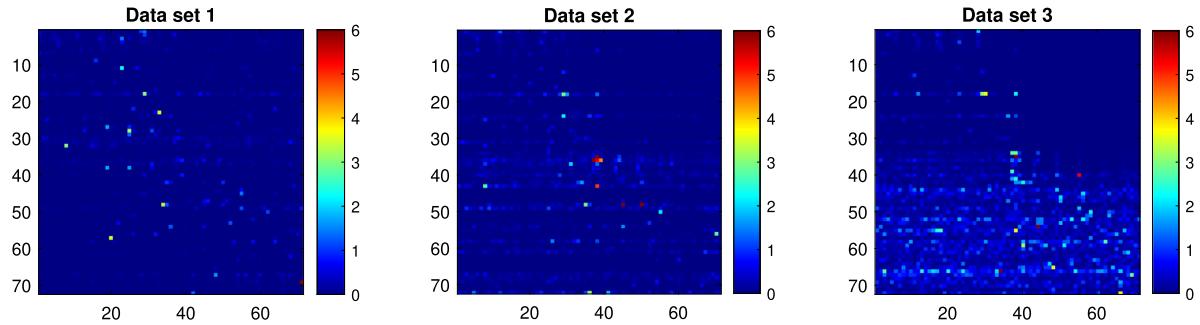

Fig. 11. Variance reduction as the ratio of the initial variance and variance after data assimilation in the case of the ensemble method. The initialization for the 3 data can be found in Fig. 6.

The inversion of $\mathbf{B}$ can be analytically calculated in a similar manner.

Appendix B. Derivation of H and (3.17)

The linearized operator H for (3.15) is a $T(r-1)\times r(r-1)$ block-diagonal matrix with $r-1$ sub-blocks, each of which has a size of $T\times r$. The jth block of H, denoted by $H(j)$, for $j=1,\ldots,r-1$ is given by

$$H(j)=\begin{bmatrix}\mathbf{y}'(0)\\ \mathbf{y}'(1)\\ \vdots\\ \mathbf{y}'(t-1)\end{bmatrix}\begin{bmatrix}\ell_{1,j} & & & \\ & \ell_{2,j} & & \\ & & \ddots & \\ & & & \ell_{r,j}\end{bmatrix}$$

where $\mathbf{y}(t)$ is defined in (2.10) and $\ell(i,j)$ is given by

$$\ell_{i,j}=\frac{e^{h_{ij}}(\ell_i-e^{h_{ij}})}{\ell_i^2}$$

and

$$\ell_i=1+\sum_{k=1}^{r-1}e^{h_{ik}}.$$

To derive (3.17), we differentiate the cost function (3.14) with respect to $\mathbf{h}$ to show that the stationary point $\mathbf{h}^*$ must satisfy

$$\mathbf{S}^{-1}(\mathbf{h}^*-\mathbf{h}^o)-\left(\frac{\partial\mathcal{H}}{\partial\mathbf{h}}\right)'\mathbf{R}^{-1}(\mathbf{y}-\mathcal{H}(\mathbf{h}^*))=0.$$

The Taylor's expansion around a point $\mathbf{h}^f$ is then used to approximate $\mathcal{H}(\mathbf{h}^*)$:

$$\mathcal{H}(\mathbf{h}^*)\approx\mathcal{H}(\mathbf{h}^f)+H(\mathbf{h}^*-\mathbf{h}^f),$$

where H is the Jacobian evaluated at the point $\mathbf{h}^f$. This leads to the stationary condition

$$\mathbf{S}^{-1}(\mathbf{h}^*-\mathbf{h}^o)-H'\mathbf{R}^{-1}\Big(\mathbf{y}-\mathcal{H}(\mathbf{h}^f)-\mathbf{H}(\mathbf{h}^*-\mathbf{h}^f)\Big)=0.$$

After a rearrangement, it can be rewritten by

$$(\mathbf{S}^{-1}+H'\mathbf{R}^{-1}H)\mathbf{h}^*-\mathbf{S}^{-1}\mathbf{h}^o-H'\mathbf{R}^{-1}(\mathbf{y}-\mathcal{H}(\mathbf{h}^f))-H'\mathbf{R}^{-1}H\mathbf{h}^f=0.$$

By adding and subtracting out $\mathbf{S}^{-1}\mathbf{h}^f$, we can rewrite the above equation as

$$\begin{aligned}\mathbf{h}^*=\mathbf{h}^f&+\mathbf{S}H'(\mathbf{R}+H\mathbf{S}H')^{-1}(\mathbf{y}-\mathcal{H}(\mathbf{h}^f))\\&+(\mathbf{S}^{-1}+H'\mathbf{R}^{-1}H)^{-1}\mathbf{S}^{-1}(\mathbf{h}^o-\mathbf{h}^f).\end{aligned}$$

Substituting $\Psi\Psi'=\mathbf{S}$ and $\mathbf{V}=H\Psi$ yields (3.17).

References

[1] X. Nie, D. Coca, A matrix-based approach to solving the inverse Frobenius–Perron problem using sequences of density functions of stochastically perturbed dynamical systems, Commun. Nonlinear Sci. Numer. Simul. 54 (2018) 248–266.

[2] X. Nie, D. Coca, Reconstruction of one-dimensional chaotic maps from sequences of probability density functions, Nonlinear Dynam. 80 (3) (2015) 1373–1390.

[3] P. Góra, A. Boyarsky, A matrix solution to the inverse Perron-Frobenius problem, Proc. Amer. Math. Soc. 118 (2) (1993) 409–414.

[4] G.G. Judge, T. Takayama, Inequality restrictions in regression analysis, J. Amer. Stat. Assoc. 61 (1966) 166–181.

[5] H. Theil, R. Guido, A quadratic programming approach to the estimation of transition probabilities, Manag. Sci. 12 (1966) 714–721.

[6] J.D. Kalbfleisch, J.F. Lawless, Least squares estimation of transition probability from aggregate data, Canadian J. Stats. 12 (3) (2008) 169–182.

[7] T.C. Lee, G.G. Judge, A. Zellner, Estimating the Parameters of the Markov Probability Model From Aggregate Time Series Data, North-Holland, 1970.

[8] M. Dellnitz, G. Froyland, O. Junge, The algorithms behind GAIO – Set oriented numerical methods for dynamical systems, in: B. Fiedler (Ed.), Ergodic Theory, Analysis, and Efficient Simulation of Dynamical Systems, Springer, 2001, pp. 145–174.

[9] L. Billings, I.B. Schwartz, Identifying almost invariant sets in stochastic dynamical systems, Chaos 18 (2008) 023122.

[10] G. Froyland, K. Padberg, Almost-invariant sets and invariant manifolds – connecting probabilistic and geometric descriptions of coherent structures in flows, Physica D 238 (16) (2009) 1507–1523.

[11] G. Froyland, S. Lloyd, N. Santitissadeekorn, Coherent sets for nonautonomous dynamical systems, Physica D 239 (2010) 1527–1541.

[12] E.M. Bollt, N. Santitissadeekorn, Applied and Computational Measurable Dynamics, SIAM, 2013.

[13] N. Santitissadeekorn, E.M. Bollt, Identifying stochastic basin hopping and mechanism by partitioning with graph modularity, Physica D 231 (2) (2007) 95–107.

[14] L. Billings, E.M. Bollt, I.B. Schwartz, Phase-space transport of stochastic chaos in population dynamics of virus spread, Phys. Rev. Lett. 88 (234101) (2002).

[15] E. Ser-Giacomi, R. Vasile, E. Hernândez-García, C. López, Most probable paths in temporal weighted networks: An application to ocean transport, Phys. Rev. E 92 (012818) (2015).

[16] I. Mezić, S. Wiggins, A method fo visualization of invariant sets of dynamical systems based on the ergodic partition, Chaos 9 (1) (1999) 213–218.

[17] G. Haller, Finding finite-time invariant manifolds in two-dimensional velocity fields, Chaos 10 (2000) 99–108.

[18] S.C. Shadden, F. Lekien, J.E. Marsden, Definition and properties of Lagrangian coherent structures from finite-time Lyapunov exponents in two-dimensional aperiodic flows, Physica D 212 (3–4) (2005) 271–304.

[19] S. Wiggins, The dynamical systems approach to Lagrangian tranport in oceanic flows, Annu. Rev. Fluid Mech. 37 (2005) 295–328.

[20] G. Haller, A variational theory of hyperbolic Lagrangian coherent structures, Physica D 240 (7) (2011) 574–598.

[21] T. Ma, E.M. Bollt, Differential geometry perspective of shape coherence and curvature evolution by finite-time nonhyperbolic splitting, SIAM J. Appl. Dyn. Syst. 13 (3) (2014) 1106–1136.

[22] A. Hadjighasem, D. Karrasch, H. Teramoto, G. Haller, Spectral clustering approach to Lagrangian vortex detection, Phys. Rev. E 93 (2016) 063107.

[23] D. Karrasch, Lagrangian transport through surfaces in volume-preserving flows, SIAM J. Appl. Math. 76 (3) (2016) 1178–1190.

[24] S. Balasuriya, N.T. Ouellette, I.I. Rypina, Generalized Lagrangian coherent structures, Physica D 372 (2018) 31–51.

[25] B. Gaveau, L. Schulman, Multiple phases in stochastic dynamics: Geometry and probabilities, Phys. Rev. E 73 (2006) 036124.

[26] T. Peacock, G. Froyland, G. Haller, Introduction to focus issue: Objective detection of coherent structures, Chaos 25 (8) (2015) 087201.

[27] G. G. Froyland, K. Padberg-Gehle, A rough-and-ready cluster-based approach for extracting finite-time coherent sets from sparse and incomplete trajectory data, Chaos 25 (8) (2015) 087406.

[28] R. Banisch, P. Koltai, Understanding the geometry of transport: Diffusion maps for Lagrangian trajectory data unravel coherent sets, Chaos 27 (2016).

[29] A. AlRahman, R. AlMomani, E.M. Bollt, Go with the flow, on Jupiter and snow. Coherence from model-free video data without trajectories, J. Nonlinear Sci. 30 (2018) 1–30.

[30] K.L. Schlueter-Kuck, J.O. Dabiri, Coherent structure colouring: Identification of coherent structures from sparse data using graph theory, J. Fluid Mech. 811 (2017) 468–486.

[31] G. Froyland, O. Junge, Robust FEM-based extraction of finite-time coherent sets using scattered, sparse, and incomplete trajectories, SIAM J. Appl. Dyn. Syst. 17 (2) (2018) 1891–1924.

[32] S. Klus, P. Koltai, C. Schütte, On the numerical approximation of the Perron-Frobenius and Koopman operator, J. Comput. Fluid Dyn. 3 (1) (2016) 51–79.

[33] S. Klus, F. Nüske, P. Koltai, H. Wu, I. Kevrekidis, C.S. abd F. Noé, Data-driven model reduction and transfer operator approximation, J. Nonlinear Sci. 28 (3) (2018) 985–1010.

[34] M. Dellnitz, O. Junge, On the approximation of complicated dynamical behaviour, SIAM J. Numer. Anal. 36 (2) (1999) 491–515.

[35] G. Froyland, Statistically optimal almost-invariant sets, Physica D 200 (2005) 205–219.

[36] G. Evensen, Data Assimilation: The Ensemble Kalman Filter, Springer-Verlag, 2006.

[37] C.H. Bishop, B.J. Etherton, S.J. Majumdar, Adaptive sampling with the ensemble transform Kalman filter. Part I: Theoretical aspects, Mon. Weather Rev. 129 (2001) 420–436.

[38] J.L. Anderson, An ensemble adjustment Kalman filter for data assimilation, Mon. Weather Rev. 129 (2001) 2884–2903.

[39] Y. Gu, D.S. Oliver, The ensemble Kalman filter for continuous updating of reservoir simulation models, J. Energy Resour. Technol. 128 (1) (2006) 79–87.

[40] M.A. Iglesias, A regularizing iterative ensemble Kalman method for PDE-constrained inverse problems, Inverse Probl. 32 (2) (2016) 025002.
[41] A.A. Emerick, A.C. Reynolds, History matching time-lapse seismic data using the ensemble Kalman filter with multiple data assimilations, Comput. Geosci. 16 (3) (2012) 639–659.
[42] P. Sakov, D.S. Oliver, L. Bertino, An iterative EnKF for strongly nonlinear systems, Month. Weather Rev. 140 (6) (2012) 1988–2004.
[43] P. Sakov, J.M. Haussaire, M. Bocquet, An iterative ensemble Kalman filter in the presence of additive model error, Quat. J. Roy. Metero. Soc. 144 (713) (2017) 1297–1309.
[44] D. Harkin, Parmeter estimation and inverse problem for reactive transport models in bioirrigated sediments (Ph.D. thesis), University of Surrey, 2020.
[45] X. Luo, I. Hoteit, Ensemble Kalman filtering with residual nudging: an extension to state estimation problems with nonlinear observation operators, Mont. Weather Rev. 142 (10) (2014) 3969–3712.